Extracellular albumin and endosomal ions prime enterovirus particles for uncoating that can be prevented by fatty acid saturation

Visa Ruokolainen[1], Aušra Domanska[2], Mira Laajala[1], Maria Pelliccia[3], Sarah J. Butcher[2], Varpu Marjomäki[1]#

[1]Department of Biological and Environmental Science, Nanoscience Center, University of Jyväskylä, PO Box 35, FI-40014 Jyväskylä, Finland

[2]Faculty of Biological and Environmental Sciences, Molecular and Integrative Bioscience Research Programme, and Helsinki Institute of Life Sciences, Institute of Biotechnology, University of Helsinki, FI-00014, Helsinki, Finland

[3]European School of Molecular Medicine (SEMM), IFOM-IEO-Campus, via Adamello 16, Milan 20139, Italy

Visa Ruokolainen and Aušra Domanska contributed equally to this article.

#Corresponding author: Varpu Marjomäki

Abstract

There is limited information about the molecular triggers leading to the uncoating of enteroviruses in physiological conditions. Using real-time spectroscopy and sucrose gradients with radioactively-labeled virus we show at 37 °C, formation of a low amount of albumin-triggered, metastable, uncoating intermediate of echovirus 1 without receptor engagement. This conversion was blocked by saturating the albumin with fatty acids. High potassium but low sodium and calcium concentrations, mimicking the endosomal environment, also induced the formation of a metastable uncoating intermediate of echovirus 1. Together, these factors boosted the formation of the uncoating intermediate and infectivity of this intermediate was retained, as judged by end-point titration. Cryo-electron microscopy reconstruction of the virions treated with albumin and high potassium, low sodium and low calcium concentrations resulted in a 3.6 Å resolution model revealing a fenestrated capsid showing 4 % expansion and loss of the pocket factor, similarly to altered (A-) particles described for other enteroviruses. The dimer interface between VP2 molecules was opened, the VP1 N-termini disordered and most likely externalised. The RNA was clearly visible, anchored to the capsid. The results presented here suggest that extracellular albumin, partially saturated with fatty acids, likely leads to the formation of the infectious uncoating intermediate prior to the engagement with the cellular receptor. In addition, changes in mono- and divalent cations, likely occurring in endosomes, promote capsid opening and genome release.

Importance

There is limited information about uncoating of enteroviruses in physiological conditions. Here, we focused on physiologically relevant factors that likely contribute to opening of echovirus 1 and other B-group enteroviruses. By combining biochemical and structural data, we show, that before entering cells, extracellular albumin is capable of priming the virus into a metastable, yet infectious intermediate state. The ionic changes that are suggested to occur in endosomes, can further contribute to uncoating and promote genome release, once the viral particle is endocytosed.

Importantly, we provide a detailed high-resolution structure of a virion after treatment with albumin and a preset ion composition, showing pocket factor release, capsid expansion and fenestration, and the clearly visible genome still anchored to the capsid. This study provides valuable information about the physiological factors that contribute to the opening of B-group enteroviruses.

Introduction

The Enterovirus B species consists of tens of clinically relevant viruses, including over 30 serotypes of echoviruses, coxsackievirus B1-B6 and A9. They can cause a wide variety of mild and severe infections and many of them are also associated with the onset of type I diabetes and coeliac disease (1-4). These viruses infect primarily gut epithelial cells and are naturally stabile in an acidic environment. This latter important feature makes the EV-B group viruses different from, for example, rhinoviruses that are known to rely on acidification during virus uncoating (5, 6).

Earlier we have shown that echovirus 1 (E1) and coxsackievirus A9 trigger a clathrin-independent entry pathway (7-10). Within 15 minutes of entry, viruses are first localized in the endosomes that develop into pH neutral multivesicular bodies. The genome uncoating continues for up to 2 hours post infection (8, 11, 12). A large number of host cell factors have been pinpointed as important regulators for the entry of enteroviruses (13). However, there is very little information on the possible extracellular and co-internalised soluble factors that potentially contribute to uncoating during infection.

Recently we described a novel uncoating intermediate particle of E1 which formed during infection and could be isolated from the cells at early stages of infection (14). This particle proved to be stable, infectious, containing all of its capsid proteins, and still capable of receptor binding (14). Previously, several studies have characterized uncoating intermediates for entero- and rhinoviruses that have been termed as A- or 135S-particles based on their altered conformation and lighter sedimentation in sucrose gradients (15). The formation of these particles has been suggested to be

induced by receptor binding (16, 17), low pH (18), or by non-physiological high temperatures (19). They have also been found to exist in purified virus preparations (20). One study showed that treatment with fatty acid free BSA converts echovirus 12 into A-particles, but the mechanism of action was not investigated further (21). In addition, there are only few studies reporting what other physiological factors, such as changes in ionic conditions, may cause on the virus particle (21-25). X-ray crystallography as well as cryo-electron microscopy (cryo-EM) and single particle reconstruction have been used to gain structural information on picornavirus particles at different stages before genome release (20, 26-33). Due to methodological challenges it has been difficult to exactly map the spatiotemporal events during the uncoating process and to link that to structural information. Furthermore, the physiological conditions in the tissues where virus infection takes place have not been carefully studied.

Here we show that albumin triggers the uncoating process of E1 at 37 °C, in a manner dependent upon the balance between fatty acids and albumin present. We further show that changes in mono- and divalent cations, likely reflecting the endosomal concentrations, also trigger a slower uncoating process of E1, which is clearly boosted by albumin.

Results

Serum at physiological temperature drives transformation from intact E1 virion to an uncoating intermediate

In this study, we investigated physiologically relevant factors that promote the uncoating process of E1. First, we noticed that in PBS buffer E1 remained infectious up to 21 days at room temperature and, remarkably, at 37 °C, still some virus stayed infectious in such conditions after 5 days (Fig. 1A). A three-hour incubation of E1 in PBS-$MgCl_2$ at 37 °C resulted in only a minor formation of empty virus particles and no formation of the uncoating intermediate, as detected by real-time fluorescent measurement in the presence or absence of RNAse (Fig. 1B). This finding was further

confirmed by gradient centrifugation of ^{35}S labelled E1 (Fig. 1C). The virus was even more stable in DPBS buffer (containing also $CaCl_2$, for buffer compositions see Table 1) throughout the 3-hour treatment (Fig. 1B). If enteroviruses are so stable, what molecules efficiently trigger uncoating in the right location, i.e. endosomes? We observed that conversion of E1 virions to intermediate particles was significantly enhanced by treating the virus with cell culture medium containing 1% serum (1% S-MEM): the SYBR Green II fluorescence increased considerably after 10 to 15 minutes incubation at +37°C, reaching maximal fluorescence around 40-50 minutes (Fig. 1D). At 45 minutes, approximately 68% of the intensity originated from intermediate particles and 32% from empty capsids (Fig. 1D). The increase of both forms was again confirmed by sucrose gradient centrifugation using ^{35}S E1 (Fig. 1E). A similar effect was also observed by fluorescence measurements of Coxsackievirus B3 and Coxsackievirus A9 (Fig. 1F) suggesting that this phenomenon was not restricted to E1. Virus conversion to the intermediate form was strictly temperature dependent, as 1% S-MEM did not induce changes in the virus capsid at room temperature but did induce the formation quickly after raising the temperature to 37 °C (Fig. 1G). Altogether, these results show that, while E1 is stable in physiological buffers, 1% bovine serum effectively induces formation of the uncoating intermediate and empty capsids at 37 °C.

Ion composition mimicking endosomal conditions also triggers the E1 uncoating process

Concerning ionic factors, uncoating of E1 and Coxsackievirus A9 is known to be independent of endosome acidification (13), which suggests that ion concentrations other than H^+, such as K^+, Na^+, Mg^{2+} and Ca^{2+} might be more important for E1 uncoating inside the endosomes. We thus chose a combination of ion concentrations based on the measurements made from endosomes (34-38) and the information provided by Scott and Gruenberg in their review on endosomal ionic conditions (39) and tested their effect on promoting E1 uncoating. The "endosomal ionic solution" used in this study contained 20 mM NaCl, 30 mM K^+, 0.5 mM $MgCl_2$ and 0.2 mM $CaCl_2$ and is referred to as

NKMC. The spectroscopy results showed that the hypotonic NKMC solution promoted a slow formation of the uncoating intermediate within a 3 h period at 37 °C, as detected by the gradual increase of fluorescence to a roughly 4-times higher level when normalized to that of the DPBS treatment (Fig. 2A). Therefore, NKMC facilitates formation of mainly porous particles most of which still contain RNA. Increasing the concentration of K^+ (60 mM) in relation to Na+ (20 mM) seemed to promote RNA release suggesting that increase of K^+ found in the endosomes may be an important factor to promote the final RNA release (Fig. 2A). We also found higher amount of RNA release when we tested omitted the divalent cations in the buffer (i.e. NK solution containing 20 mM NaCl and 30 mM K^+ without Mg^{2+} or Ca^{2+}). Without Mg^{2+} or Ca^{2+}, the fluorescence signal was mainly comprised of released RNA indicating the presence of mainly empty capsids (Fig. 2A). This is in line with the previously observed stabilizing effect of divalent cations on viral particles (24, 40-45) . The stabilizing effect of divalent cations was further verified by complementing the NK solution with different concentrations of Ca^{2+} or Mg^{2+} ions. Similarly to NK solution without divalent cations, concentrations of 0.002 and 0.02 mM Ca^{2+}, 100-fold and 10-fold dilutions of Ca^{2+} compared to NKMC respectively, as well as 0.005 and 0.05 mM Mg^{2+}, 100-fold and 10-fold dilutions of Mg^{2+} compared to NKMC respectively, mainly caused formation of empty virions (Fig 2B and C). In contrast, the presence 0.2 mM Ca^{2+} or 0.5 mM Mg^{2+} in NK solution prevented RNA release from a significant number of the virions (Fig 2B and C, black lines).

We also tested different concentrations of sodium and potassium ranging between their extra- and intracellular values (extracellular concentrations roughly 140 mM Na^+ and 5 mM K^+ versus intracellular 5 mM Na^+ and 140 mM K^+). The concentration of Mg^{2+} and Ca^{2+} were kept at their cytoplasmic values of 0.8 mM and 0.2 µM, respectively, while we changed Na^+ and K^+ concentrations step-by-step from 5 mM to 140 mM and 140 mM to 5 mM, respectively. The results showed that, at 37 °C, cytoplasmic ionic concentrations caused a clear increase in the number of empty virus particles: RNA release started already within 15 min (Fig. 2D). This suggests that the

intracellular ion concentrations, 140 mM K^+, 5mM Na^+, 0.5 mM $MgCl_2$ and 0.2 µM Ca^{2+} are effective in promoting RNA release. Notably, the extracellular concentrations of Na^+ (high) and K^+ (low) resulted in formation of empty particles in the presence of intracellular Mg^{2+} (0.5mM) and Ca^{2+} (0.2µM) concentrations (Fig. 2D). The concentrations of K^+ and Na^+ between the extremes were less effective at promoting RNA release (Fig. 2E-F).

In summary, the ionic conditions found in endosomes, with lowered Na^+ and Ca^{2+} and higher K^+ concentrations as compared to the extracellular space, trigger a slow uncoating process. Even further reduction in the Ca^{2+} concentration and increase in K^+ concentration, as may happen in the endosomes, facilitates also the RNA release from the virions.

Albumin triggers the E1 uncoating process

Comparison of 1% S-MEM and MEM without serum clearly showed that serum triggered the uncoating process resulting in an increase of both the uncoating intermediate and empty virus (Fig. 3A). We then tested if serum would have any additive effect when administrated in the NKMC solution. We observed a clear increase in the rate of the fluorescence signal appearance: with NKMC, the maximal fluorescence signal was reached only at the end of the 3 h measurement, whereas in the presence of 1% serum this time was shortened to about 30 min (Fig. 3B). Interestingly, with 1% serum, the amount of RNA released from the virions decreased and the intermediate particles remained stable throughout the measurement.

In order to narrow down the serum components responsible for the boosting effect, we focused on albumin, as it is the most abundant protein in serum (46). As 1% serum corresponds to approximately 0.04% albumin solution, we decided to use 0.01-0.1% BSA concentrations to see if albumin was responsible for the changes that we observed with 1% S-MEM. As it is known that albumin is a high affinity fatty acid carrier in the blood (46), and the lipid moiety, typically palmitate

(47), present in the hydrophobic pocket of many enteroviruses is important for the virion stability (15), we tested also fatty acid free BSA (faf-BSA) in our experiments.

The spectroscopy measurements showed that both BSA and faf-BSA triggered the uncoating process in MEM in a similar manner to 1% S-MEM (Fig. 3A and 3C), suggesting that the major factor in serum initiating the uncoating process is indeed the serum albumin. Moreover, both albumin forms promoted serum-like effects in NKMC too (Fig. 3D). After observing, that BSA and faf-BSA resulted in similar results as serum in both isotonic MEM and hypotonic NKMC, we tested faf-BSA in DPBS and saw that it induced the uncoating process similarly to MEM (Fig. 3E). Spectroscopy analysis of the virus treated with EM buffer prepared for cryoEM imaging, showed a high amount of the uncoating intermediate particles (Fig. 3E).

Since albumin appeared to be the major factor inducing and boosting the virus priming, we tested if addition of fatty acids would prevent the observed effect. We started with conditions that most efficiently caused RNA release: We treated the ^{35}S-labelled E1 with NK solution supplemented with 0.1% faf-BSA (Fig. 3F, red curve peak fractions 4-9). The presence of approximately 100-fold molar excess of palmitate (400 µM) with respect to the amount of albumin in the assay, fully protected the E1 virions from the structural changes as detected by sucrose gradient analysis (Fig. 3F, blue curve).

We next explored in more detail the molar ratio between BSA and virus required for efficient triggering of the uncoating process. We found that albumin to virion ratio of 1200:1 (comparable to 0,01% faf-BSA solution with 1µg of E1 used in spectroscopy assays), which corresponds to albumin ratio to hydrophobic pocket of 20:1, efficiently triggered the formation of the uncoating intermediate (Fig. 3G). In contrast, albumin to virion ratio of 120:1 showed only a mild effect and ratio 17:1 induced no changes when compared to the control condition (data not shown). The virus treatment with albumin did not significantly increase the amount of empty viruses.

Then we tested the concentration of free fatty acids needed to prevent the uncoating process. Adding increasing amounts of palmitate to the faf-BSA virus mixture reduced the formation of uncoating intermediate and concomitantly increased the amount of intact virions (Fig. 3G). Full protection against uncoating was gained by adding a 50-fold molar excess of palmitate with respect to the faf-BSA molecules, whereas a 20-fold excess showed an intermediate effect (Fig. 3G). The effect of a 10-fold excess was still notable but an equimolar ratio showed no protection (data not shown).

These results show that albumin is the major component of the serum that triggers the uncoating process. It further stresses the fact that the net balance between fatty acids and albumin is important in enterovirus particle uncoating.

Structural details of the treated virion

Having ascertained the physiological factors that could reproducibly start the uncoating process, we studied the treated virions by negative staining as well as by cryoEM and single particle reconstruction. Negatively-stained preparations of cryoEM buffer treated sample revealed three distinct forms of E1: intact, intermediate and empty particles (Fig. 4A). In the EM buffer treated virus sample, 29% of particles were intact, 65% were intermediate and 6% were empty (out of 2108), whereas in non-treated sample the percentages were 95%, 4% and 1% (out of 2624), respectively. In cryoEM micrographs we could not distinguish between intact and the intermediate particles by eye, but after image analysis and classification 70 % of all particles were intermediate (23983 out of 34160) processed from the treated sample's micrographs (Fig. 4B). Thus, the reconstruction of the treated particle described below represents the averaged structure for the most populated viral particle in the treated sample. Two-dimensional averages of the control and treated particles clearly show the density for both the capsid and RNA (Fig 4C).

Icosahedral reconstruction of the intact E1 virus from the control sample's cryoEM micrographs to 3.5 Å resolution, was similar to the published X-ray structure PDB ID 1EV1 (48) . The atomic

model fitted into the intact E1 reconstruction included the lipid factor in the lipid pocket and density for all four capsid proteins, VP1, VP2, VP3 and VP4 (Table 3, Fig. 4D, F, G, H and Fig. 5A-C) (48). The RMSD compared to the X-ray structure was 0.77 Å. The intact E1 reconstruction shows icosahedrally-averaged RNA density which has not been reported earlier (Fig. 4F and H, Fig. 5A). The majority of the RNA follows the outline of the capsid and is distributed at a distance of 0 – 10 Å from the inner capsid surface, with the highest density between radii 94 and 113 Å (from the virion center). The RNA has clear connections around the two-fold axes of symmetry to Trp 38 of VP2 (Fig. 5A). In addition, Arg 13 and Arg 27 of VP1 as well as a poorly resolved VP4 loop contact the RNA density. Similar RNA-capsid interactions involving VP2 Trp 38 and VP1 N-terminus have been described in intact rhinovirus particles (30).

In comparison, the 3.6 Å resolution treated particle reconstruction has undergone a 4% expansion (Fig. 4E, I, J, K). It was possible to model most of the VP1, VP2 and VP3, but none of VP4 in to the reconstruction (Table 3 and Fig. 5D-F). The atomic modelling revealed that the capsid expansion occurred through rotation and outwards translation of the capsid proteins VP1, VP2 and VP3. This results in a fenestrated capsid, with prominent holes on the edges of the capsid close to the two-fold axes of symmetry at the VP2 dimer interface, a hallmark of A-particles described for other enteroviruses (Fig. 4J and Fig. 6A-B). The atomic model emphasizes these holes, somewhat artificially, as not all the electron density has been accounted for (Fig. 6B). The pocket factor has been released (Fig. 5E and F). The GH loop on VP1, thought to be important in pocket factor release has moved, collapsing the pocket. The RNA is clearly visible, its average conformation has changed, but it still maintains connections to the capsid via VP2 Trp 38, Glu 40 and Tyr 41 (Fig. 5D). The contacts mediated by the VP1 N-termini and VP4 have been lost in the treated particle, but new connections appeared via the N-termini of VP3 below the five-fold vertices. In the control particle these VP3 termini interact with VP4. Similar RNA-capsid interactions mediated by VP2 Trp 38 and VP3 N-termini were seen in expanded rhinovirus particles (30). The averaged RNA still

follows the profile of the inner surface of the capsid, but has moved outwards (Fig. 4, 5 and 6), with the highest density between radii 102 and 122Å. Thus, the RNA is less densely packed in the treated intermediate particle.

Besides the poorly-ordered density inside the capsid assigned to viral RNA, the difference map between the control reconstruction and the atomic model of intact E1 showed only a small unassigned density in the capsid protein region at the three-fold axes of symmetry (Fig. 6C). This unassigned density could be attributed to six un-modelled residues of the VP2 N-terminus (Fig. 6C, red arrows in the inset). The difference map between the treated particle reconstruction and atomic model, revealed, less-well ordered, lower resolution density near the two-fold axes spanning the capsid from the interior to the exterior, and at the five-fold axes on the particle surface (Fig. 6D). The first modelled residue of the VP1 N-terminus (Asn 55) lies in close proximity to the unassigned density near the two-fold axis inside the particle and therefore, the unassigned density could be the VP1 N-termini now traversing the capsid and exposed on the surface of the treated capsid similarly to the interpretation for expanded particles of other enteroviruses (Fig. 6D, red arrows in the inset) (20, 26, 49). In addition, part of this poorly-ordered density seen on the exterior could be attributed to a flexible VP3 loop (residues Thr 175 – Asp 183). The poorly defined density seen at the five-fold axes on the capsid surface is most likely attributed to disordered loops in VP1 (residues Thr 131 – Asn 136). Although VP4 could not be modelled in the density, its partial presence in the treated sample was confirmed by autoradiography (Fig. 7). Moreover, the treated virus sample showed about 2 logs lower infectivity (decrease from 8.23×10^{11} to 1.01×10^{10}) confirming our previously published data for the E1 uncoating intermediate particle (14). Hence, VP4 could contribute to both the poorly-ordered density on the inside of the capsid close to the vertices, attributed primarily to RNA, as well as to the density spanning the capsid. In corroboration of this finding, the presence of a tiny amount of VP4 was recently reported in A-particles of enterovirus D68 induced by acid treatment (49).

Discussion

We have shown previously that during entry into cells, E1 undergoes structural changes that were first discovered as an increased permeability to the small molecule dye, SYBR Green II, and Cs-ions (14). Here, we showed by cryoEM that temperature-dependent structural changes, under physiological conditions, involved expansion of the virus particle, loosening of the genome packing, loss of the lipid factor and formation of larger openings at the VP2 dimer interface, explaining the increased permeability to the small molecular dye and the resistance to RNase treatment observed previously (14). We also showed by spectroscopy that serum-priming of coxsackievirus B3 and coxsackievirus A9 caused similar changes in permeability to that of E1 suggesting that also other enteroviruses behave similarly (Fig. 1F).

Our *in vitro* experiments demonstrated two important factors in the serum and extracellular space affecting the integrity and the dynamics of E1 virion at 37 °C, albumin and fatty acids, one of the most abundant components in the serum and interstitial fluids. Albumin concentration in serum has been reported as 640 µM (46) and the albumin bound fatty acids concentration ranging from 200 to 700 µM in serum (50). As mentioned before, albumin serves as the major fatty acid carrier in the blood with two to three high affinity and four to five intermediate affinity binding sites for fatty acids (46). Also, the fatty acid binding capacity of BSA and faf-BSA have been measured to be around 4.8 moles and 7 moles per mole albumin, respectively (51). The measurements further showed that BSA is approximately 50% occupied by serum fatty acids, meaning that roughly 50% of the fatty acid binding capacity is still left (51) . Furthermore, both Penn et al. (51) and Van der Vusse (46) showed that bovine and human albumin have very similar fatty acid binding capacities making bovine albumin a good surrogate for human albumin. These data provide further support, that in physiological conditions, BSA is not saturated with fatty acids. Thus, the most likely explanation for the increased intermediate particle formation at low fatty acid concentration is the partitioning of the fatty acid moiety from the capsid into a more hydrophobic environment, such as

Journal of Virology

into the fatty acid binding sites on the albumin. Higher temperature will result in higher mobility of the fatty acid. Furthermore, the fatty acid saturation level of albumin has a great effect on capsid stability. This was demonstrated by the prevention of virus expansion and RNA release using increasing concentrations of palmitate in comparison to albumin (Figs. 3E and 3F). Considering the observed molar excess of fatty acids required to prevent formation of albumin-induced intermediate particle (Fig. 3F), and the approximately 1:1 ratio of albumin and fatty acids observed in serum, it seems probable that in physiological conditions, the albumin present outside the cells starts the uncoating process. The ability of faf-BSA to induce echovirus A-particle formation was previously shown using a radioactive gradient, however the nature of this process was not studied further (21). Our results here explain the mechanism by which faf-BSA induces uncoating in enteroviruses, such as echoviruses and coxsackieviruses. Moreover, we suggest that the loss of the pocket factor likely precedes receptor binding, promoting the formation of an infectious intermediate particle already in the extracellular space.

The expansion of E1 capsid does not affect the receptor, α_2I-domain, binding site (14, 52). However, the expansion does cause changes in the amino acid composition exposed on the capsid surface such as the exposure of the VP1 N-terminus, which may also give rise to new secondary receptor-binding sites. If some lipid factors would still be bound to the capsid in the endosome initially, it could well exchange into the hydrophobic environment of the endosomal membrane that would extract the lipid factor from the capsid. In support of this hypothesis, albumin readily donates fatty acids to other fatty acid binding proteins in the vicinity of the plasma membrane. Furthermore, the binding and release of the lipid factor in enteroviruses is known to be a dynamic process (53, 54). A potential endosomal membrane protein that could help to sequester the lipid factor is the lipid-modifying enzyme PLA2G16 (55). It is thought to affect the insertion of VP4 into the endosomal membrane, but could potentially help to sequester the lipid factor too (56).

Journal of Virology

314 The next and final step in picornavirus uncoating is the RNA release. Accumulated results on
315 CVA9 and E1 uncoating show that it starts as early as 15 to 30 min post infection and the extent of
316 uncoating increases strongly until 1 to 2 h post-infection (57, 58). However, the first signs of
317 replication, including -RNA and +RNA production occur as late as 2 h post-infection (59). This
318 suggests that the ambient endosomal ion conditions develop gradually to better promote the
319 uncoating and the final RNA release into the cytoplasm. Current information on the intra-
320 endosomal ionic changes over time suggests that the sodium and calcium concentrations in
321 endosomes decrease during their maturation and potassium concentration rises relative to the
322 extracellular values (39). Our results demonstrated that a combination of low sodium and calcium
323 and elevated potassium in the presence of physiological magnesium concentration was also able to
324 trigger the uncoating process, but, however, it was more rapid in the presence of albumin (Fig. 3B
325 and 3D). Furthermore, in addition to the formation of the uncoating intermediate, the right
326 combination of ions led to significantly more efficient RNA release (Fig. 2A) that could be further
327 increased with faf-BSA (Fig. 3E, fluorescence data not shown). In the lack of thorough absolute
328 ionic concentration measurements inside the endosomes, the present study may underestimate the
329 complexity of the and actual combination of the ions present. No ions have been resolved in the X-
330 ray structure of E1, so we cannot directly interpret the effects of the ions on the capsid or the RNA
331 stability. However, both K^+ and Mg^{2+} ions can stabilize RNA tertiary structures (60). Thus, we
332 hypothesize that changes in these ions may contribute to the expansion of the RNA, providing an
333 additional force to promote conformational change in the capsid and eventual release of the RNA in
334 the endosome. Changes in the Ca^{2+} and Na^+ ion concentrations probably affect the protein stability,
335 through electrostatic interactions. Ca^{2+} has been shown to be important for the capsid stability of
336 many viruses (24, 40-44).
337 The RNA-capsid interactions were resolved in structures of A-particles published for several
338 enteroviruses like enterovirus 71, coxsackievirus A16 and rhinovirus 2, suggesting their importance

339 in assisting RNA release (20, 30, 31). The genome is unique within the capsid, nevertheless, in some
340 picornaviruses the RNA is so well ordered, that individual bases can be identified ranging from one
341 base to several (61-66). Here, the icosahedral reconstructions also showed for the first-time details of
342 the RNA, though not resolved to the atomic level, inside the intact E1 particle and in the uncoating
343 intermediate structure. The RNA has a high density in proximity to the intact capsid, which
344 suggests high occupancy, and the probable interaction of the RNA with both the ordered capsid
345 proteins (notably with VP1, VP4 and VP2 shown in Fig. 5A) and their disordered termini (67).
346 Trp38 in VP2, highly concerved residue in picornaviruses, points towards ordered RNA (61-66).
347 This interaction between the RNA and capsid is directly adjacent to the major fenestrations that
348 appear in the treated capsid, where the RNA has moved radially outwards, maintaining this specific
349 interaction (Fig. 5D). Interestingly, this RNA-capsid interaction is in proximity to the N-terminus of
350 VP1 that appears to be extruded from the treated capsid, similarly to the VP1 in expanded
351 poliovirus, coxsackievirus A16 and enterovirus D68 (20, 26, 49). VP4 could not be identified in the
352 reconstruction, suggesting that it is no longer icosahedrally-ordered or the occupancy is much
353 reduced as suggested also by autoradiography. This implies that the RNA interaction with the
354 capsid via VP4 under the vertices has significantly altered compared to the intact particle (Fig. 5).
355 VP4 may have collapsed into the density attributed to RNA that is still prominent below the VP3
356 annulus at the vertices (Fig. 4 and 5). Changes in the RNA packaging density and its interaction
357 with the capsid proteins, along with the expansion of the particle are probably also responsible for
358 the increase in permeability to dye.
359 Altogether, our results suggest that, based on the dynamic nature of albumin-mediated fatty acid
360 binding, and the fact that both albumin and fatty acids are present outside cells, the majority of the
361 enterovirus particles may reside in a triggered, intermediate, metastable state before entering cells.
362 According to our results, the albumin-triggered intermediate state is likely to lead to more efficient

363 RNA release when it is further affected by the ambient concentrations of monovalent and divalent
364 cations in endosomes.

365 ## Materials and methods

366 ### E1 production and purification

367 E1 was produced and purified as described earlier (14). Confluent 5-layer bottles of green monkey
368 kidney (GMK) cells, obtained from the American Type Culture Collection (ATCC), were infected
369 with E1 (Farouk strain, ATCC), for 16-20 hours at 37 °C, 5% CO_2. After infection, the cells and
370 media were collected and lysed with three freeze-thaw cycles. The lysate was pelleted by
371 centrifugation with a JA-10 rotor (6080 rpm, 30 min, +4 °C) after which the supernatant was
372 precipitated for 16-20 h at + 4°C using polyethylene glycol 6000 (Sigma Aldrich, Saint Louis,
373 Missouri, US) (8% wt/vol) and NaCl (2.2% wt/vol). The precipitated supernatant was then
374 centrifuged with a JA-10 rotor (8000 rpm, 45 min, +4 °C) and the resulting pellet was dissolved
375 into R buffer (10 mM Tris-HCl (pH 7.5), 200 mM $MgCl_2$, 10 % (wt/vol) glycerol). For disrupting
376 the remaining cellular membranes, 0.3 % (wt/vol) sodium deoxycholate (Sigma Aldrich) and 0.6%
377 (vol/vol) Nonidet P-40 (Sigma Aldrich) were mixed with the supernatant and incubated for 30 min
378 on ice. The remaining debris was pelleted by centrifuging in a TX-200 rotor (4700 rpm, 15 min, +
379 4°C), and the resulting supernatant was loaded on top of 10 ml linear 10-40% (wt/volume) sucrose
380 gradients in R buffer. The gradients were ultracentrifuged in an SW-41 rotor (30000 rpm, 3 h, +
381 4°C) and fractioned into 500 µl aliquots. The optical density at 260 nm of each fraction was
382 measured with a NanoDrop 1000 Spectrophotometer (Thermo Scientific, Waltham, Massachusetts,
383 US), to identify fractions containing virus. These fractions were dialyzed against 2 mM $MgCl_2$-
384 phosphate buffered saline (PBS-$MgCl_2$) in a Spectra/Por Micro Float-A-Lyzer with Biotech
385 cellulose ester membranes and 300 kDa cut off (Spectrum Laboratories Inc. USA) at +4 °C. Finally,
386 the viruses were pelleted by ultracentrifugation using a 70Ti rotor (35000 rpm, 2 h, +4 °C) and

resuspended in PBS-$MgCl_2$. Several purified virus batches were used ranging between 0.5-1.3 mg/ml and 1 x 10^{11}-1 x 10^{12} pfu/ml.

^{35}S E1 production and purification

^{35}S labelled E1 for gradient analysis was produced in GMK cells as described earlier (14) . Semi-confluent cell culture bottles were washed at 37 °C for 15 min with PBS and infected with E1 (Farouk strain; ATCC) using low-methionine-cysteine medium supplemented with 1% FBS for three hours. After this the media was changed into the above-mentioned media supplemented with 50 µCi/ml of [^{35}S]methionine-cysteine and the infection was allowed to proceed 16-24 h until nearly all of the cells were detached. The cells were lysed via 3 freeze-thaw cycles and the cell debris was pelleted using a TX-200 rotor (4000 rpm for 15 min, +4°C). The supernatant was further treated with 0.3% (wt/vol) sodium deoxycholate and 0.6 % (vol/vol) Nonidet P-40 for 30 min on ice and the supernatant was further cleared by centrifuging (TX-200, 4700 rpm, 15min, +4 °C). The supernatant was loaded onto the top of a 2ml 40 % sucrose cushion at +4 °C. The cushions were ultracentrifuged at 30000 rpm (SW-41) for 2.5 hours at +4 °C after which the liquid above the cushion and one 500 µl fraction from the cushion were discarded and the three next 500 µl fractions were collected. These fractions were diluted into PBS-2mM $MgCl_2$ and the virus was pelleted by centrifuging 35000 rpm (Ti70) 2-3 h at +4 °C, after which the pellet was resuspended into 1.5 ml of PBS-$MgCl_2$ and the different virus populations were further separated in a 5-20% sucrose gradient in R-buffer via gradient centrifugation (35000 rpm, SW41, 2 h, +4°C). The virus-containing fractions were identified via liquid scintillation counting (Perkin Elmer, Waltham, Massachusetts, US). The three fractions containing the highest amount of intact virus particles were again collected and pelleted as above. The resulted pellet was dissolved into 400 µl of PBS-$MgCl_2$, divided into smaller aliquots and stored at -80°C after determination of CPM/µl of the 35S E1 stock.

CVB3 and CVA9 production and purification

CVB3 (ATCC, Nancy strain) and CVA9 (ATCC, Griggs strain) were purified in a similarly to E1, except it was separated in 5-20% sucrose gradient. From the gradient, fractions 1-10 were discarded and 11-20 collected. The collected fractions were diluted with PBS-$MgCl_2$ into a final volume of 25ml and concentrated as described for E1.

End-point dilution assay

The end-point dilution infection assay was done as described earlier (68). Shortly, GMK cells were cultured in 10% serum-containing MEM and infected with E1 in a dilution series in the presence of 1% serum. Typically, after 3 days of infection at +37 °C the 96-well plate was stained with 50 µl of crystal violet stain (8.3 mM crystal violet, 45 mM $CaCl_2$, 10% ethanol, 18.5% formalin and 35 mM Tris base) for 10 minutes. $TCID_{50}$ was determined by calculating the numbers of infected and uninfected wells for the eight replicates in one 96-well plate at each dilution. Pfu/ml was calculated by multiplying the $TCID_{50}$/ml value with 0.7 according to the Poisson distribution estimation.

Real-time fluorescence uncoating measurements

The measurements were done using a PerkinElmer 2030 Multilabel Reader Victor X4 with F485 lamp filter and F535 emission filter and one second counting time. In each measurement 1 µg of non-labelled virus (corresponding to 0.77-2 µl of PBS-$MgCl_2$, depending on the stock concentration) was treated in 100 µl of the buffer described in each experiment in a single well of 96 well plate (Sarstedt, Nümbrecht, Germany) in the presence of 10X SYBR Green II fluorescent dye. The composition of the buffers is presented in table **1**. All of the buffers were neutral in pH ranging between 7.18-7.44. Where indicated, RNAse A was added to the wells at a final concentration of 10 µg ml^{-1}. By adding RNAse to the assay, we distinguished between the fluorescence originating from the porous intermediate particles i.e. from RNA inside the virus capsid (protected from the RNAse activity), and the fluorescence of RNA released from the particles (sensitive to RNAse treatment) indicating the presence of empty particles. Intact virion is inaccessible to the dye and thus gives a low fluorescence signal (14). For each virus treatment a

436 corresponding blank well with all other factors except virus was also measured and the fluorescence
437 was subtracted to eliminate fluorescence originating from other factors than the virus. Each well
438 was measured either every minute or every other minute for a three-hour time period at 37 °C if not
439 otherwise stated. The plate was prepared on ice, from where it was placed into a preheated
440 measurement chamber. The results were processed and plotted using Microsoft excel. The error
441 bars represented the standard error of the mean from a minimum of five technical replicates from at
442 least two separate biological replicates. In all graphs the amount of fluorescence is normalized to
443 the end fluorescence value of the control, three-hour DPBS treatment.

444 **Gradient analysis**

445 1 µl (approximately 10,000-80,000 CPM) of 35S E1 together with 1 µg of non-radioactive E1 was
446 treated for 1 h at +37 °C in 100 µl of the relevant buffer. The samples were then cooled on ice and
447 loaded on to a cooled 10-ml linear 5 to 20% sucrose gradient. The gradients were centrifuged using
448 an SW-41 rotor (35,000 rpm, 2 h, +4°C) and 500 µl fractions were collected and mixed with
449 scintillation cocktail (Ultima Gold MW, Perkin Elmer). The samples were analyzed using Tri-Carb
450 2910 TR (Perkin Elmer) and plotted in excel. Every treatment was repeated at least once and similar
451 effects were observed.

452 In the albumin-virus-fatty acid ratio experiment, the molarity of E1 was calculated using molecular
453 weight estimation of 8 MDa for E1 which resulted in 1.25 nM E1 solution with 1 µg of virus in
454 100 µl of buffer. According to this, 1200 times higher faf-BSA (Sigma Aldrich, in ddH_2O)
455 concentration (1.5 µM, 1200 albumins per virus) of faf-BSA was used for 20:1 ratio of albumin
456 molecules to virus pocket factors and 120 times higher concentration for 2:1 ratio. 17 times higher
457 concentration was used for 2:1 ratio between the albumin`s high to medium affinity fatty acid
458 binding sites (7 per albumin) vs. virus pocket factors (60 per virus). Palmitate (Sigma Aldrich) from
459 15.2 mM stock in 50% MeOH was added in either 20:1 or 50:1 ratio into the 1.5 µM faf-BSA
460 solution.

EM sample preparation, imaging, particle processing and model building

Virus sample for cryoEM and negative staining was prepared as follows. Purified E1 in PBS-$MgCl_2$ buffer at a concentration of 1.27 µg/µl was mixed with 20 mM NaCl, 30 mM K^+ and 0.01 % faf-BSA buffer giving a final concentration of 0.1 µg/ul virus, 29 mM NaCl, 28 mM K^+, 0.145 mM $MgCl_2$ and 0.0093% faf-BSA (EM buffer) and incubated for 1 h at 37 °C. The uncoating intermediate formation was confirmed by spectroscopy measurement (Fig. 3E). Control samples were prepared from purified E1 in PBS-$MgCl_2$.

Butwar-coated copper grids were glow discharged (EMS/SC7620 Mini sputter coater), after which the virus sample was added and incubated for 15 s. The excess virus was blotted away and the grids were negatively-stained using phosphotungstic acid (H_2O, pH 7.4) for 60 seconds and the excess stain was blotted away. The samples were stored overnight at RT before imaging with a JEM-1400 (JEOL) transmission electron microscope (80kV, Olympus SIS Quemesa bottom-mounted 11 Megapixel CCD camera, 12,000-40,000 x magnification).

Sample volumes of 3 µl of control or EM buffer-treated E1 particle were applied to glow-discharged Quantifoil holey carbon R2/2 grids and vitrified using a custom-made manual plunger. The vitrified samples were imaged on a 200 kV Talos Arctica microscope equipped with a Falcon III direct electron detector at a nominal magnification of 120,000 x corresponding to a calibrated pixel size of 1.24 Å. Each exposure was 47.8 s long and collected as a movie containing 30 frames with an accumulated dose of 30 e/$Å^2$ using Thermo Fisher Scientific's automatic data acquisition software.

Dose-fractionated image stacks were aligned using MotionCor2 (69). The contrast transfer function parameters for each micrograph were estimated using Gctf (70). Images containing drift or astigmatism were discarded. Particle selection, 2D classification, initial model generation and 3D classification were performed using RELION 2.1 (71). Final 3D refinement followed by sharpening (B-factor -70 $Å^2$) of 45309 intact particles from control sample (~45% of total particles) resulted in

a 3.5 Å resolution map. After applying the same procedure to 14615 uncoating intermediate particles from treated sample (~59% of total particles), a 3.6 Å resolution map was generated.

Model building

A crystal structure of the E1 virion (PDB ID: 1EV1) served as an initial starting model for the intact E1 particle (48). An initial atomic model for the uncoating intermediate particle was generated using the I-TASSER server (72) based on the crystal structure of the CVA16 uncoating intermediate (PDB ID: 4JGY) (20, 73). The atomic coordinates of the initial models were docked manually into the electron density maps using UCSF Chimera and further optimized using the 'Fit in Map' command (74). In the case of the intact particle, one residue (Cys7) was added to the VP2 N-terminus of 1EV1 model using Coot 0.8.8 and the fit was further optimized using molecular dynamics flexible fitting (MDFF) software used along with NAMD and VMD (69-72) (75). A scale factor of 1 was used to weigh the contribution of the cryo-EM map to the overall potential function used in MDFF. Simulations included 10,000 steps of minimization and 100,000 steps of molecular dynamics under implicit solvent conditions with secondary structure restraints in place. The atomic model of the uncoating intermediate particle was refined in Coot 0.8.8 and this served as an input for MDFF, NAMD and VMD software (75-78). Simulations with scale factor of 1 included 20,000 steps of minimization and 100,000 steps of molecular dynamics under implicit solvent conditions with secondary structure restraints in place. To minimize atom clashes in the atomic model processed in MDFF, seven asymmetric units were simultaneously refined in MDFF using the same secondary structure restraints as above. To analyse unassigned density in intact or treated virion reconstruction, the atomic model was converted to 3.5 (intact) or 3.6 (treated) Å resolution electron density map using the 'molmap' command in UCSF Chimera. The map generated for the accounted density was then subtracted from the reconstruction using the 'vop subtract' command in UCSF Chimera. The treated particle expansion was estimated by measuring the particle diameter between the five-fold vertices in intact and treated virions.

511 **Gel separation of viral proteins and autoradiography**

512 1 µg of non-radioactive E1 with 1 µl of ^{35}S E1 (approximately 10,000-80,000 CPM) was treated for
513 1 h at 37 °C in EM buffer. Non-treated virus was used as a VP4 detachment negative control and
514 virus incubated for 10 minutes at 50°C was used as a positive control. Samples were dialysed
515 against 1 liter of PBS-$MgCl_2$ for 40 minutes using Slide-A-Lyzer mini dialysis device with 10 kDa
516 cut off (Thermo Fisher Scientific) to remove the possibly detached VP4 from the samples. The
517 samples were boiled for 10 min with the sample buffer and ran to 4-20 gradient gel (MINI-
518 PROTEAN TGX precast gel, Bio-Rad Laboratories, Inc., Hercules, California, US). Precision plus
519 protein standard 10-250 kDa (Bio-Rad Laboratories, Inc., Hercules, California, US) was used to
520 distinguish the molecular weight. The gel was fixed in 30% methanol, 10% acetic acid and treated
521 with autoradiography enhancer (Enlightning, Perkin Elmer). The gel was dried at +70 °C for 2 h
522 (Gel dryer 583, Bio-Rad Laboratories, Inc., Hercules, California, US) and subjected to
523 autoradiography. Protein bands were analyzed using ImageJ gel analyzer tool.

524 **Data availability**

525 The final density maps have been deposited in the Electron Microscopy Databank (EMDB) with
526 accession codes EMD-4903 (control E1) and EMD-0565 (expanded E1). The atomic models have
527 been deposited in the Worldwide Protein Databank (wwPDB) with accession codes 6RJF (control
528 E1) and 6O06 (expanded E1). The raw data have been deposited in the EMPIAR database with
529 deposition ID 414.

530

531

532 ## Acknowledgments

533 We thank Benita Löflund and Pasi Laurinmäki (University of Helsinki), as well as Instruct-FI, the
534 Biocenter Finland National cryo-electron microscopy unit, HILiFE-Institute of Biotechnology, and
535 the CSC-IT Center for Science Ltd. for providing technical assistance and facilities to carry out the

work. We also thank Tino Kantoluoto (University of Jyväskylä) for virus production and purification. This work was supported by the Academy of Finland (275199 and 315950 to S.J.B.) (257125 to V.M.), the Sigrid Juselius Foundation (S.J.B.) and Jane and Aatos Erkko foundation (V.M.).

V.M., V.R., A.D., and S.J.B. conceptualized the study. M.P., A.D., V.R., S.J.B., and V.M. curated data. M.P., V.R., M.L., A.D, S.J.B., and V.M., developed the methodology. V.R. and A.D. validated the data. V.R. and A.D visualized the data. V.R. M.L., A.D, S.J.B., and V.M. wrote the manuscript. V.M. and S.J.B. acquired funding. A.D., S.J.B., and V.M. supervised the study. S.J.B. and V.M. served as project administrators.

References

1. **Kahrs, CR, Chuda, K, Tapia, G, Stene, LC, Marild, K, Rasmussen, T, Ronningen, KS, Lundin, KEA, Kramna, L, Cinek, O, Stordal, K.** 2019. Enterovirus as trigger of coeliac disease: nested case-control study within prospective birth cohort. Bmj. **364:**l231. doi: 10.1136/bmj.l231 [doi].

2. **Roivainen, M, Klingel, K.** 2009. Role of enteroviruses in the pathogenesis of type 1 diabetes. Diabetologia. **52:**995-996. doi: 10.1007/s00125-009-1332-9 [doi].

3. **Laitinen, OH, Honkanen, H, Pakkanen, O, Oikarinen, S, Hankaniemi, MM, Huhtala, H, Ruokoranta, T, Lecouturier, V, Andre, P, Harju, R, Virtanen, SM, Lehtonen, J, Almond, JW, Simell, T, Simell, O, Ilonen, J, Veijola, R, Knip, M, Hyoty, H.** 2014. Coxsackievirus B1 is

associated with induction of beta-cell autoimmunity that portends type 1 diabetes. Diabetes. **63:**446-455. doi: 10.2337/db13-0619 [doi].

4. **Sioofy-Khojine, AB, Lehtonen, J, Nurminen, N, Laitinen, OH, Oikarinen, S, Huhtala, H, Pakkanen, O, Ruokoranta, T, Hankaniemi, MM, Toppari, J, Vaha-Makila, M, Ilonen, J, Veijola, R, Knip, M, Hyoty, H.** 2018. Coxsackievirus B1 infections are associated with the initiation of insulin-driven autoimmunity that progresses to type 1 diabetes. Diabetologia. **61:**1193-1202. doi: 10.1007/s00125-018-4561-y [doi].

5. **Nurani, G, Lindqvist, B, Casasnovas, JM.** 2003. Receptor priming of major group human rhinoviruses for uncoating and entry at mild low-pH environments. J. Virol. **77:**11985-11991.

6. **Brabec, M, Baravalle, G, Blaas, D, Fuchs, R.** 2003. Conformational changes, plasma membrane penetration, and infection by human rhinovirus type 2: role of receptors and low pH. J. Virol. **77:**5370-5377.

7. **Karjalainen, M, Kakkonen, E, Upla, P, Paloranta, H, Kankaanpaa, P, Liberali, P, Renkema, GH, Hyypia, T, Heino, J, Marjomaki, V.** 2008. A Raft-derived, Pak1-regulated entry participates in alpha2beta1 integrin-dependent sorting to caveosomes. Mol. Biol. Cell. **19:**2857-2869. doi: 10.1091/mbc.E07-10-1094 [doi].

8. **Karjalainen, M, Rintanen, N, Lehkonen, M, Kallio, K, Maki, A, Hellstrom, K, Siljamaki, V, Upla, P, Marjomaki, V.** 2011. Echovirus 1 infection depends on biogenesis of novel multivesicular bodies. Cell. Microbiol. **13:**1975-1995. doi: 10.1111/j.1462-5822.2011.01685.x [doi].

578 9. **Marjomaki, V, Pietiainen, V, Matilainen, H, Upla, P, Ivaska, J, Nissinen, L, Reunanen, H,**
579 **Huttunen, P, Hyypia, T, Heino, J.** 2002. Internalization of echovirus 1 in caveolae. J. Virol.
580 **76:**1856-1865.

581 10. **Heikkila, O, Susi, P, Tevaluoto, T, Harma, H, Marjomaki, V, Hyypia, T, Kiljunen, S.** 2010.
582 Internalization of coxsackievirus A9 is mediated by {beta}2-microglobulin, dynamin, and Arf6 but
583 not by caveolin-1 or clathrin. J. Virol. **84:**3666-3681. doi: 10.1128/JVI.01340-09 [doi].

584 11. **Soonsawad, P, Paavolainen, L, Upla, P, Weerachatyanukul, W, Rintanen, N, Espinoza, J,**
585 **McNerney, G, Marjomaki, V, Cheng, RH.** 2014. Permeability changes of integrin-containing
586 multivesicular structures triggered by picornavirus entry. PLoS One. **9:**e108948. doi:
587 10.1371/journal.pone.0108948 [doi].

588 12. **Huttunen, M, Waris, M, Kajander, R, Hyypia, T, Marjomaki, V.** 2014. Coxsackievirus A9
589 infects cells via nonacidic multivesicular bodies. J. Virol. **88:**5138-5151. doi: 10.1128/JVI.03275-
590 13 [doi].

591 13. **Marjomaki, V, Turkki, P, Huttunen, M.** 2015. Infectious Entry Pathway of Enterovirus B
592 Species. Viruses. **7:**6387-6399. doi: 10.3390/v7122945 [doi].

593 14. **Myllynen, M, Kazmertsuk, A, Marjomaki, V.** 2016. A Novel Open and Infectious Form of
594 Echovirus 1. J. Virol. **90:**6759-6770. doi: 10.1128/JVI.00342-16 [doi].

595 15. **Tuthill, TJ, Groppelli, E, Hogle, JM, Rowlands, DJ.** 2010. Picornaviruses. Curr. Top.
596 Microbiol. Immunol. **343:**43-89. doi: 10.1007/82_2010_37 [doi].

597 16. **Casasnovas, JM, Springer, TA.** 1994. Pathway of rhinovirus disruption by soluble
598 intercellular adhesion molecule 1 (ICAM-1): an intermediate in which ICAM-1 is bound and RNA
599 is released. J. Virol. **68:**5882-5889.

600 17. **Kaplan, G, Freistadt, MS, Racaniello, VR.** 1990. Neutralization of poliovirus by cell
601 receptors expressed in insect cells. J. Virol. **64:**4697-4702.

602 18. **Prchla, E, Kuechler, E, Blaas, D, Fuchs, R.** 1994. Uncoating of human rhinovirus serotype 2
603 from late endosomes. J. Virol. **68:**3713-3723.

604 19. **Curry, S, Chow, M, Hogle, JM.** 1996. The poliovirus 135S particle is infectious. J. Virol.
605 **70:**7125-7131.

606 20. **Ren, J, Wang, X, Hu, Z, Gao, Q, Sun, Y, Li, X, Porta, C, Walter, TS, Gilbert, RJ, Zhao, Y,**
607 **Axford, D, Williams, M, McAuley, K, Rowlands, DJ, Yin, W, Wang, J, Stuart, DI, Rao, Z,**
608 **Fry, EE.** 2013. Picornavirus uncoating intermediate captured in atomic detail. Nat. Commun.
609 **4:**1929. doi: 10.1038/ncomms2889 [doi].

610 21. **Ward, T, Powell, RM, Chaudhry, Y, Meredith, J, Almond, JW, Kraus, W, Nelsen-Salz, B,**
611 **Eggers, HJ, Evans, DJ.** 2000. Fatty acid-depleted albumin induces the formation of echovirus A
612 particles. J. Virol. **74:**3410-3412.

613 22. **Lonberg-Holm, K, Gosser, LB, Shimshick, EJ.** 1976. Interaction of liposomes with subviral
614 particles of poliovirus type 2 and rhinovirus type 2. J. Virol. **19:**746-749.

615 23. **Cords, CE, James, CG, McLaren, LC.** 1975. Alteration of capsid proteins of coxsackievirus
616 A13 by low ionic concentrations. J. Virol. **15:**244-252.

617 24. **Wetz, K, Kucinski, T.** 1991. Influence of different ionic and pH environments on structural
618 alterations of poliovirus and their possible relation to virus uncoating. J. Gen. Virol. **72 (Pt**
619 **10):**2541-2544. doi: 10.1099/0022-1317-72-10-2541 [doi].

620 25. **Ward, T, Powell, RM, Evans, DJ, Almond, JW.** 1999. Serum albumin inhibits echovirus 7
621 uncoating. J. Gen. Virol. **80 (Pt 2):**283-290. doi: 10.1099/0022-1317-80-2-283 [doi].

622 26. **Butan, C, Filman, DJ, Hogle, JM.** 2014. Cryo-electron microscopy reconstruction shows
623 poliovirus 135S particles poised for membrane interaction and RNA release. J. Virol. **88:**1758-
624 1770. doi: 10.1128/JVI.01949-13 [doi].

625 27. **Lin, J, Cheng, N, Hogle, JM, Steven, AC, Belnap, DM.** 2013. Conformational shift of a major
626 poliovirus antigen confirmed by immuno-cryogenic electron microscopy. J. Immunol. **191:**884-891.
627 doi: 10.4049/jimmunol.1202014 [doi].

628 28. **Lee, H, Shingler, KL, Organtini, LJ, Ashley, RE, Makhov, AM, Conway, JF, Hafenstein,**
629 **S.** 2016. The novel asymmetric entry intermediate of a picornavirus captured with nanodiscs. Sci.
630 Adv. **2:**e1501929. doi: 10.1126/sciadv.1501929 [doi].

631 29. **Organtini, LJ, Makhov, AM, Conway, JF, Hafenstein, S, Carson, SD.** 2014. Kinetic and
632 structural analysis of coxsackievirus B3 receptor interactions and formation of the A-particle. J.
633 Virol. **88:**5755-5765. doi: 10.1128/JVI.00299-14 [doi].

634 30. **Pickl-Herk, A, Luque, D, Vives-Adrian, L, Querol-Audi, J, Garriga, D, Trus, BL,**
635 **Verdaguer, N, Blaas, D, Caston, JR.** 2013. Uncoating of common cold virus is preceded by RNA
636 switching as determined by X-ray and cryo-EM analyses of the subviral A-particle. Proc. Natl.
637 Acad. Sci. U. S. A. **110:**20063-20068. doi: 10.1073/pnas.1312128110 [doi].

638 31. **Shingler, KL, Yoder, JL, Carnegie, MS, Ashley, RE, Makhov, AM, Conway, JF,**
639 **Hafenstein, S.** 2013. The enterovirus 71 A-particle forms a gateway to allow genome release: a
640 cryoEM study of picornavirus uncoating. PLoS Pathog. **9:**e1003240. doi:
641 10.1371/journal.ppat.1003240 [doi].

642 32. **Strauss, M, Filman, DJ, Belnap, DM, Cheng, N, Noel, RT, Hogle, JM.** 2015. Nectin-like
643 interactions between poliovirus and its receptor trigger conformational changes associated with cell
644 entry. J. Virol. **89:**4143-4157. doi: 10.1128/JVI.03101-14 [doi].

645 33. **Lin, J, Lee, LY, Roivainen, M, Filman, DJ, Hogle, JM, Belnap, DM.** 2012. Structure of the
646 Fab-labeled "breathing" state of native poliovirus. J. Virol. **86:**5959-5962. doi: 10.1128/JVI.05990-
647 11 [doi].

648 34. **Gerasimenko, JV, Tepikin, AV, Petersen, OH, Gerasimenko, OV.** 1998. Calcium uptake via
649 endocytosis with rapid release from acidifying endosomes. Curr. Biol. **8:**1335-1338. doi: S0960-
650 9822(07)00565-9 [pii].

651 35. **Christensen, KA, Myers, JT, Swanson, JA.** 2002. pH-dependent regulation of lysosomal
652 calcium in macrophages. J. Cell. Sci. **115:**599-607.

653 36. **Weinert, S, Jabs, S, Supanchart, C, Schweizer, M, Gimber, N, Richter, M, Rademann, J,**
654 **Stauber, T, Kornak, U, Jentsch, TJ.** 2010. Lysosomal pathology and osteopetrosis upon loss of
655 H+-driven lysosomal Cl- accumulation. Science. **328:**1401-1403. doi: 10.1126/science.1188072
656 [doi].

657 37. **Hara-Chikuma, M, Yang, B, Sonawane, ND, Sasaki, S, Uchida, S, Verkman, AS.** 2005.
658 ClC-3 chloride channels facilitate endosomal acidification and chloride accumulation. J. Biol.
659 Chem. **280:**1241-1247. doi: M407030200 [pii].

660 38. **Steinberg, BE, Huynh, KK, Brodovitch, A, Jabs, S, Stauber, T, Jentsch, TJ, Grinstein, S.**
661 2010. A cation counterflux supports lysosomal acidification. J. Cell Biol. **189:**1171-1186. doi:
662 10.1083/jcb.200911083 [doi].

663 39. **Scott, CC, Gruenberg, J.** 2011. Ion flux and the function of endosomes and lysosomes: pH is
664 just the start: the flux of ions across endosomal membranes influences endosome function not only
665 through regulation of the luminal pH. Bioessays. **33:**103-110. doi: 10.1002/bies.201000108 [doi].

666 40. **Pfeiffer, P, Herzog, M, Hirth, L.** 1976. RNA viruses: stabilization of brome mosaic virus.
667 Philos. Trans. R. Soc. Lond. B. Biol. Sci. **276:**99-107.

668 41. **Hull, R.** 1978. The stabilization of the particles of turnip rosette virus. III. Divalent cations.
669 Virology. **89:**418-422. doi: 0042-6822(78)90184-8 [pii].

670 42. **Bishop, NE, Anderson, DA.** 1997. Early interactions of hepatitis A virus with cultured cells:
671 viral elution and the effect of pH and calcium ions. Arch. Virol. **142:**2161-2178.

672 43. **Kivela, HM, Mannisto, RH, Kalkkinen, N, Bamford, DH.** 1999. Purification and protein
673 composition of PM2, the first lipid-containing bacterial virus to be isolated. Virology. **262:**364-374.
674 doi: 10.1006/viro.1999.9838 [doi].

675 44. **Sherman, MB, Guenther, RH, Tama, F, Sit, TL, Brooks, CL, Mikhailov, AM, Orlova, EV,**
676 **Baker, TS, Lommel, SA.** 2006. Removal of divalent cations induces structural transitions in red
677 clover necrotic mosaic virus, revealing a potential mechanism for RNA release. J. Virol. **80:**10395-
678 10406. doi: JVI.01137-06 [pii].

679 45. **Speir, JA, Munshi, S, Wang, G, Baker, TS, Johnson, JE.** 1995. Structures of the native and
680 swollen forms of cowpea chlorotic mottle virus determined by X-ray crystallography and cryo-
681 electron microscopy. Structure. **3:**63-78. doi: S0969-2126(01)00135-6 [pii].

682 46. **van der Vusse, G J.** 2009. Albumin as fatty acid transporter. Drug Metab. Pharmacokinet.
683 **24:**300-307. doi: JST.JSTAGE/dmpk/24.300 [pii].

684 47. **Smyth, M, Pettitt, T, Symonds, A, Martin, J.** 2003. Identification of the pocket factors in a
685 picornavirus. Arch. Virol. **148:**1225-1233. doi: 10.1007/s00705-002-0974-4 [doi].

686 48. **Filman, DJ, Wien, MW, Cunningham, JA, Bergelson, JM, Hogle, JM.** 1998. Structure
687 determination of echovirus 1. Acta Crystallogr. D Biol. Crystallogr. **54:**1261-1272.

688 49. **Liu, Y, Sheng, J, van Vliet, A L W, Buda, G, van Kuppeveld, F J M, Rossmann, MG.** 2018.
689 Molecular basis for the acid-initiated uncoating of human enterovirus D68. Proc. Natl. Acad. Sci.
690 U. S. A. **115:**E12209-E12217. doi: 10.1073/pnas.1803347115 [doi].

691 50. **Abdelmagid, SA, Clarke, SE, Nielsen, DE, Badawi, A, El-Sohemy, A, Mutch, DM, Ma,**
692 **DW.** 2015. Comprehensive profiling of plasma fatty acid concentrations in young healthy Canadian
693 adults. PLoS One. **10:**e0116195. doi: 10.1371/journal.pone.0116195 [doi].

694 51. **Penn, AH, Dubick, MA, Torres Filho, IP.** 2017. Fatty Acid Saturation of Albumin Used in
695 Resuscitation Fluids Modulates Cell Damage in Shock: in vitro Results Using a Novel Technique to
696 Measure Fatty Acid Binding Capacity. Shock. **48:**449-458. doi: 10.1097/SHK.0000000000000865
697 [doi].

698 52. **Xing, L, Huhtala, M, Pietiainen, V, Kapyla, J, Vuorinen, K, Marjomaki, V, Heino, J,**
699 **Johnson, MS, Hyypia, T, Cheng, RH.** 2004. Structural and functional analysis of integrin alpha2I
700 domain interaction with echovirus 1. J. Biol. Chem. **279:**11632-11638. doi:
701 10.1074/jbc.M312441200 [doi].

702 53. **Trigatti, BL, Gerber, GE.** 1995. A direct role for serum albumin in the cellular uptake of long-
703 chain fatty acids. Biochem. J. **308 (Pt 1):**155-159.

704 54. **Martikainen, M, Salorinne, K, Lahtinen, T, Malola, S, Permi, P, Hakkinen, H,**
705 **Marjomaki, V.** 2015. Hydrophobic pocket targeting probes for enteroviruses. Nanoscale. **7:**17457-
706 17467. doi: 10.1039/c5nr04139b [doi].

707 55. **Staring, J, von Castelmur, E, Blomen, VA, van den Hengel, L G, Brockmann, M, Baggen,**
708 **J, Thibaut, HJ, Nieuwenhuis, J, Janssen, H, van Kuppeveld, FJ, Perrakis, A, Carette, JE,**
709 **Brummelkamp, TR.** 2017. PLA2G16 represents a switch between entry and clearance of
710 Picornaviridae. Nature. **541:**412-416. doi: 10.1038/nature21032 [doi].

711 56. **Baggen, J, Thibaut, HJ, Strating, J R P M, van Kuppeveld, F J M.** 2018. The life cycle of
712 non-polio enteroviruses and how to target it. Nat. Rev. Microbiol. **16:**368-381. doi:
713 10.1038/s41579-018-0005-4 [doi].

714 57. **Siljamaki, E, Rintanen, N, Kirsi, M, Upla, P, Wang, W, Karjalainen, M, Ikonen, E,**
715 **Marjomaki, V.** 2013. Cholesterol dependence of collagen and echovirus 1 trafficking along the
716 novel alpha2beta1 integrin internalization pathway. PLoS One. **8:**e55465. doi:
717 10.1371/journal.pone.0055465 [doi].

718 58. **Huttunen, M, Turkki, P, Maki, A, Paavolainen, L, Ruusuvuori, P, Marjomaki, V.** 2017.
719 Echovirus 1 internalization negatively regulates epidermal growth factor receptor downregulation.
720 Cell. Microbiol. **19:**10.1111/cmi.12671. Epub 2016 Oct 20. doi: 10.1111/cmi.12671 [doi].

721 59. **Upla, P, Marjomaki, V, Nissinen, L, Nylund, C, Waris, M, Hyypia, T, Heino, J.** 2008.
722 Calpain 1 and 2 are required for RNA replication of echovirus 1. J. Virol. **82:**1581-1590. doi:
723 JVI.01375-07 [pii].

724 60. **Draper, DE.** 2004. A guide to ions and RNA structure. Rna. **10:**335-343.

725 61. **Hendry, E, Hatanaka, H, Fry, E, Smyth, M, Tate, J, Stanway, G, Santti, J, Maaronen, M,**
726 **Hyypia, T, Stuart, D.** 1999. The crystal structure of coxsackievirus A9: new insights into the
727 uncoating mechanisms of enteroviruses. Structure. **7:**1527-1538. doi: S0969-2126(00)88343-4 [pii].

728 62. **Muckelbauer, JK, Kremer, M, Minor, I, Diana, G, Dutko, FJ, Groarke, J, Pevear, DC,**
729 **Rossmann, MG.** 1995. The structure of coxsackievirus B3 at 3.5 A resolution. Structure. **3:**653-
730 667. doi: S0969-2126(01)00201-5 [pii].

731 63. **Arnold, E, Rossmann, MG.** 1990. Analysis of the structure of a common cold virus, human
732 rhinovirus 14, refined at a resolution of 3.0 A. J. Mol. Biol. **211:**763-801. doi: 0022-
733 2836(90)90076-X [pii].

734 64. **Hadfield, AT, Lee, W, Zhao, R, Oliveira, MA, Minor, I, Rueckert, RR, Rossmann, MG.**
735 1997. The refined structure of human rhinovirus 16 at 2.15 A resolution: implications for the viral
736 life cycle. Structure. **5:**427-441. doi: S0969-2126(97)00199-8 [pii].

737 65. **Kalynych, S, Palkova, L, Plevka, P.** 2015. The Structure of Human Parechovirus 1 Reveals an
738 Association of the RNA Genome with the Capsid. J. Virol. **90:**1377-1386. doi: 10.1128/JVI.02346-
739 15 [doi].

740 66. **Domanska, A, Flatt, JW, Jukonen, JJJ, Geraets, JA, Butcher, SJ.** 2019. A 2.8-Angstrom-
741 Resolution Cryo-Electron Microscopy Structure of Human Parechovirus 3 in Complex with Fab
742 from a Neutralizing Antibody. J. Virol. **93:**10.1128/JVI.01597-18. Print 2019 Feb 15. doi: e01597-
743 18 [pii].

744 67. **Shakeel, S, Evans, JD, Hazelbaker, M, Kao, CC, Vaughan, RC, Butcher, SJ.** 2018.
745 Intrinsically-disordered N-termini in human parechovirus 1 capsid proteins bind encapsidated RNA.
746 Sci. Rep. **8:**5820-018. doi: 10.1038/s41598-018-23552-7 [doi].

747 68. **Schmidtke, M, Schnittler, U, Jahn, B, Dahse, H, Stelzner, A.** 2001. A rapid assay for
748 evaluation of antiviral activity against coxsackie virus B3, influenza virus A, and herpes simplex
749 virus type 1. J. Virol. Methods. **95:**133-143. doi: S0166093401003056 [pii].

750 69. **Zheng, SQ, Palovcak, E, Armache, JP, Verba, KA, Cheng, Y, Agard, DA.** 2017.
751 MotionCor2: anisotropic correction of beam-induced motion for improved cryo-electron
752 microscopy. Nat. Methods. **14:**331-332. doi: 10.1038/nmeth.4193 [doi].

753 70. **Zhang, K.** 2016. Gctf: Real-time CTF determination and correction. J. Struct. Biol. **193:**1-12.
754 doi: 10.1016/j.jsb.2015.11.003 [doi].

755 71. **Scheres, SH.** 2012. RELION: implementation of a Bayesian approach to cryo-EM structure
756 determination. J. Struct. Biol. **180:**519-530. doi: 10.1016/j.jsb.2012.09.006 [doi].

757 72. **Yang, J, Yan, R, Roy, A, Xu, D, Poisson, J, Zhang, Y.** 2015. The I-TASSER Suite: protein
758 structure and function prediction. Nat. Methods. **12:**7-8. doi: 10.1038/nmeth.3213 [doi].

759 73. **Roy, A, Kucukural, A, Zhang, Y.** 2010. I-TASSER: a unified platform for automated protein
760 structure and function prediction. Nat. Protoc. **5:**725-738. doi: 10.1038/nprot.2010.5 [doi].

761 74. **Pettersen, EF, Goddard, TD, Huang, CC, Couch, GS, Greenblatt, DM, Meng, EC, Ferrin,**
762 **TE.** 2004. UCSF Chimera--a visualization system for exploratory research and analysis. J. Comput.
763 Chem. **25:**1605-1612. doi: 10.1002/jcc.20084 [doi].

764 75. **Emsley, P, Lohkamp, B, Scott, WG, Cowtan, K.** 2010. Features and development of Coot.
765 Acta Crystallogr. D Biol. Crystallogr. **66:**486-501. doi: 10.1107/S0907444910007493 [doi].

766 76. **Humphrey, W, Dalke, A, Schulten, K.** 1996. VMD: visual molecular dynamics. J. Mol.
767 Graph. **14:**33-8, 27. doi: 0263785596000185 [pii].

768 77. **Phillips, JC, Braun, R, Wang, W, Gumbart, J, Tajkhorshid, E, Villa, E, Chipot, C, Skeel,**
769 **RD, Kale, L, Schulten, K.** 2005. Scalable molecular dynamics with NAMD. J. Comput. Chem.
770 **26:**1781-1802. doi: 10.1002/jcc.20289 [doi].

771 78. **Trabuco, LG, Villa, E, Mitra, K, Frank, J, Schulten, K.** 2008. Flexible fitting of atomic
772 structures into electron microscopy maps using molecular dynamics. Structure. **16:**673-683. doi:
773 10.1016/j.str.2008.03.005 [doi].

774 79. **Kucukelbir, A, Sigworth, FJ, Tagare, HD.** 2014. Quantifying the local resolution of cryo-EM
775 density maps. Nat. Methods. **11:**63-65. doi: 10.1038/nmeth.2727 [doi].

776

777 ## Figure legends

778

779 Fig. 1. Echovirus 1 stability. (A) Infectivity of E1 after 1, 5, 15 or 21 days in PBS at +37 °C or
780 room temperature. (B) Fluorescence measurement of SGII-dye in the presence of 1 µg E1 in PBS-
781 $MgCl_2$ (black line) and DPBS (red line) with (dotted line) or without (solid line) RNAse during 3 h
782 at 37 °C. (C) 5-20% sucrose gradient separation of ^{35}S-labeled E1 when treated for 1 h at +37 °C in
783 PBS-$MgCl_2$ (blue) vs. non-treated virus (black). The amount of different virus populations is shown
784 in the inset. (D) Fluorescence measurement of SGII-dye in the presence of 1 µg E1 in 1% S-MEM
785 at 37 °C (Black lines). In gray, as an example, results of the same virus measurements (solid line)
786 before subtracting the blank measurements (dotted line). In the presented results of 1% S-MEM
787 (black line), and in all of the presented fluorescent results in this paper, the blank, which contains
788 all other factors except the virus (gray dotted line), is subtracted from the measurement with virus
789 (gray solid line). (E) 5-20% sucrose gradient separation of ^{35}S-labeled E1 when treated for 0-60 min
790 at +37 °C in 1% S-MEM. The amount of different virus populations is shown in the inset. (F)
791 Fluorescence measurement of SGII-dye in the presence of 1 µg of CVB3 or CVA9 in 1% MEM at

+37 °C during 3 h. (G) Fluorescence measurement of SGII-dye in the presence of 1 µg E1 in 1% S-MEM at room temperature (23 °C) for 60 minutes after which the multilabel reader heater was turned to 37 °C for 90 minutes. The transition from room temperature to 37 °C lasted about 12 minutes.

In all of the fluorescence measurements, in this and other figures, the Y-axis is normalized to the final fluorescence value of the control DPBS treatment (Fig. 1B, red solid line). Treatments in each buffer with and without RNAse are marked with same colour but dotted and solid lines, respectively. All fluorescence measurements are averages of minimum five measurements and the presented error bars are ±standard error of the mean.

Fig. 2. Virus stability in NK solution with different amounts of K^+, Mg^{2+} (M) and Ca^{2+} (C) at 37 °C. (A) Fluorescence measurement of SGII-dye in the presence of 1 µg E1 in NKMC, containing 30 mM K phosphate (black lines), NKMC with higher, 60 mM K phosphate (red lines) and NK (i.e. without Mg^{2+} and Ca^{2+}, blue lines) solutions. (B) Fluorescence measurement of SGII-dye in the presence of 1 µg E1 in NK solution with different amounts of $CaCl_2$ (C = 200 µM, 0.1C = 20 µM, 0.01C = 2 µM). (C) Fluorescence measurement of SGII-dye in the presence of 1 µg E1 in NK solution with different amounts of $MgCl_2$ (M = 500 µM, 0.1M = 50 µM, 0.01M = 5 µM). D) Fluorescence measurement of SGII-dye at 37 °C in the presence of 1 µg E1 in either intra- and extracellular Na^+ and K^+ concentrations, combined with intracellular 800 µM $MgCl^2$ and 0.2 µM $CaCl^2$ concentrations. (E-F) Fluorescence measurement of SGII-dye at +37 °C in the presence of 1 µg E1 in varying Na^+ and K^+ concentrations between intra- and extracellular values, but constant intracellular 800 µM $MgCl^2$ and 0.2 µM $CaCl^2$ concentrations.

816 Fig. 3. Serum and albumin promote virus opening at 37 °C. (A) Fluorescence measurement of SGII-
817 dye in the presence of 1 µg E1 in MEM and 1% S-MEM. (B) Fluorescence measurement of SGII-
818 dye in the presence of 1 µg E1 in NKMC and 1% S-NKMC. (C) Fluorescence measurement of
819 SGII-dye in the presence of 1 µg E1 in MEM supplemented with 0.01% BSA or faf-BSA. (D)
820 Fluorescence measurement of SGII-dye in the presence of 1 µg E1 in NKMC solution
821 supplemented with 0,01% BSA or faf-BSA. (E) Fluorescence measurement of SGII-dye in the
822 presence of 1 µg E1 in DPBS supplemented with 0.01% faf-BSA and in EM buffer. (F) Effect of
823 faf-BSA and fatty acids on virus uncoating and priming using 5-20% sucrose gradient analysis of
824 metabolically labelled ^{35}S E1. Non-treated virus (black line) in comparison to fully opened virus
825 (red line; 1 h incubation with 0.1% faf-BSA NK at 37 °C) and fatty acid-rescued virus after addition
826 of 400 µM palmitate (blue). (G) Virus treated for 1 h at 37 °C in DPBS (black line) in comparison
827 to DPBS supplemented with 1.5 µM faf-BSA (20:1 ratio of faf-BSA to virus hydrophobic pockets,
828 red line), or, in addition to 1.5 µM faf-BSA, with increasing (20:1 and 50:1) molar ratio of
829 palmitate to the faf-BSA (light blue and dark blue lines, respectively).
830
831 Fig. 4. Electron Microscopy and Cryo-EM reconstructions of E1 intact and treated virions.
832 (A) Negative stain of E1 after 1 h treatment at 37 °C with 29 mM NaCl, 28 mM K, 0.145 mM
833 $MgCl_2$, 0.0093% faf-BSA. (B) Cryo-electron micrographs of non-treated (control) E1 and E1 after
834 similar treatment to (A). (A & B) The white arrow indicates intact virion, the red arrow indicates
835 empty, and the green arrow indicates intermediate particle. Scale bar is 50 nm. (C) Example of 2D
836 class averages showing intact (control, n=16298), treated (treated, n=2015) and empty class
837 averages (n=212), where n is the number of particles contributing to the average shown. Box size is
838 496 Å (D) Fourier shell correlation curves for the control E1 reconstruction, giving a resolution of
839 3.5 Å with a cutoff of 0.143. (E) Fourier shell correlation curves for the treated particle
840 reconstruction giving a resolution of 3.6 Å with a cutoff of 0.143. (D &E) Corrected (black),

841 unmasked (green), masked (blue) and phase randomized masked (red) maps (71). (F) Control E1
842 reconstruction central plane. Pentagon, triangle, and oval indicate five-fold, three-fold and two-fold
843 symmetry axes, respectively. (G) Radially coloured isosurface representation of the control E1
844 reconstruction viewed down a two-fold axis of symmetry at 1.5 SD above the mean. Pentagons and
845 triangle mark five-fold and three-fold axes, respectively. Two-fold axis is in the middle between the
846 two marked five-fold axes. (H) Control E1 coloured by local resolution (79). (I) Treated particle
847 reconstruction central plane. (J) Isosurface representation of treated particle viewed down a two-
848 fold axis of symmetry at 1.5 SD above the mean. (G & J) Radially coloured according to the colour
849 key in (G). (K) Treated particle coloured by local resolution. (J & K) Resolution coloured according
850 to the colour key in (H).
851
852 Fig. 5. Comparison of reconstructions and atomic models of control and treated E1 virions. (A) Slab
853 of the virion atomic model (1EV1) (48) shown in ribbon, fitted into the control E1 density on the
854 left-hand side. Most of the capsid density is accounted for by the atomic model, but the inner
855 density from the RNA is not. The upper right inset highlights the structure of one pentamer with
856 VP4. The lower right inset highlights the interaction of the RNA and VP2 Trp38 next to the two-
857 fold. (B) Section of control E1 reconstruction revealing the pocket and the lipid factor. (C) The
858 same as in (B) with the atomic model fitted. (D) Slab of the treated atomic model (wwPDB
859 deposition ID 6O06) shown in ribbon, fitted into the treated particle density on the left-hand side.
860 Most of the capsid density is accounted for by the atomic model, but the inner density from the
861 RNA is not. The position of the RNA has moved radially outwards as the capsid expanded,
862 maintaining the two-fold connections. The upper right inset highlights the structure of one pentamer
863 without VP4 modelled as there was no apparent density for it. The lower right inset highlights the
864 interaction of the RNA and VP2 Trp38 next to the two-fold. (E) Section of treated particle
865 reconstruction revealing the collapsed pocket and no evident density for the lipid factor. (F) The

same as in (E) with the atomic model fitted. (A-F) EM density shown in transparent grey, lipid factor EM density in orange, VP1 (blue ribbon), VP2 (cyan ribbon), VP3 (green ribbon), VP4 (yellow ribbon), lipid factor (orange stick). (B & E) Orange oval indicates the corresponding positions of the pocket.

Fig. 6. Treated particle expansion and unmodelled cryo-EM density. (A) Atomic model of control E1 seen along two-fold axis. (B) Atomic model of the treated intermediate virion seen along two-fold axis showing opening between two VP2 helices. (C) Unmodelled cryo-EM density of control E1 (grey isosurface). Inset shows unmodelled density at the three-fold axis. Red arrows indicate N-termini of VP2 (Cys 7) in the vicinity of unmodelled density blob. Triangle indicates three-fold symmetry axis. (D) Unmodelled cryo-EM density of the treated virion (grey isosurface). Inset shows unmodelled density spanning the capsid near two-fold axis. Red arrows indicate N-termini of VP1 (Asn 55) in the vicinity of the unmodelled density spanning the capsid. Pentagon and oval indicate five-fold and two-fold symmetry axes, respectively. (A-D) VP1 (blue), VP2 (cyan), VP3 (green), VP4 (yellow), lipid factor (orange).

Fig 7. Autoradiography observation of ^{35}S-labelled VP4 protein. Metabolically labelled E1, non-treated, heated to 50°C for 10 minutes, and EM buffer treated sample.

Tables

Table 1. Exact compositions of the buffers used in the paper. The concentrations are in mM.

Buffer/ compoound	NaCl	Na_2HPO_4	Total Na	KCl	KH_2PO_4	K_2HPO_4	Total K	$MgCl_2$	$CaCl_2$	faf-BSA	pH
PBS	137	8	145	3	2		5				7.34
PBS-$MgCl_2$	137	8	145	3	2		5	2			7.22
DPBS	138	8.1	146.1	2.7	1.5		4.2	0.5	0.9		7.25
NKMC	20		20		6	12	30	0.5	0.2		7.18
NK	20		20		6	12	30			0.0093%	7.25
EM buffer	29		29		5.6	11.2	28	0.145			7.28

Table 2. Summary of cryo-EM data collection, refinement, and validation statistics.

	Treated E1	Control E1
Data collection		
Voltage (kV)	200	200
Electron exposure (e-/Å^2 X s)	30	30
Pixel size (Å)	1.24	1.24
Number of micrographs	1,246	979
Reconstruction		
Number of particles	14615	45309
B factor (Å^2)	-70	-70
FSC threshold	0.143	0.143
Resolution (Å)	3.6	3.5
Model building		
VP1 (full protein 281 aa)	55 – 130 and 137 – 280	1 – 281
VP2 (full protein 261 aa)	12 – 54 and 58 – 261	7 – 261
VP3 (full protein 239 aa)	3 – 174 and 184 – 237	1 – 239
VP4 (full protein 68 aa)	none	1 – 14 and 22 – 68
Model validation		
MolProbity score	1.25/100th percentile*	1.08/100th percentile**
Ramachandran outliers (%)	4.3	2.06
Poor rotamers (%)	1.7	1.24
Clashscore	0	0

*(N=342, 3.25Å - 3.85Å); **(N=27675, 0Å - 99Å)

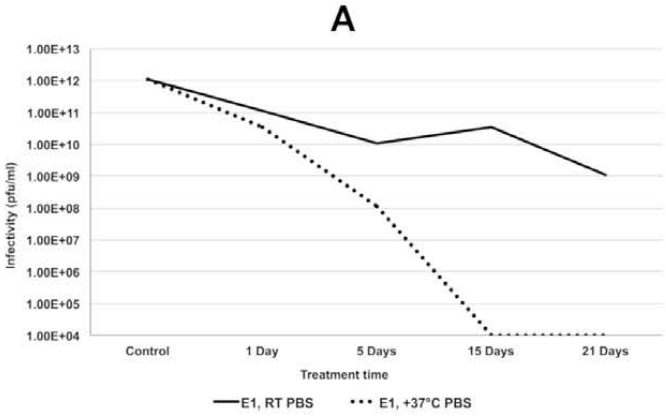

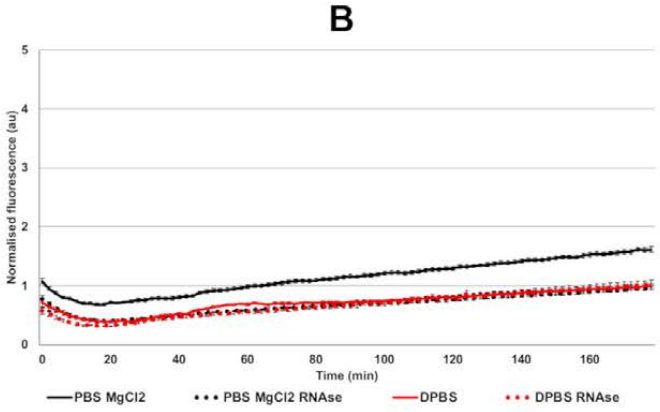

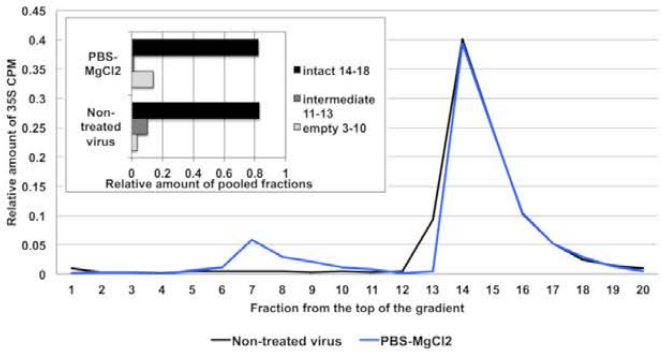

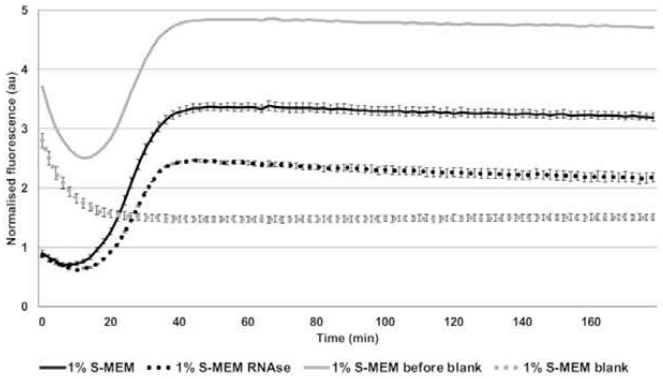

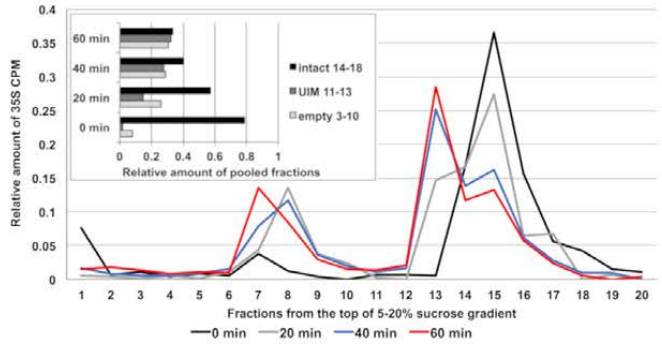

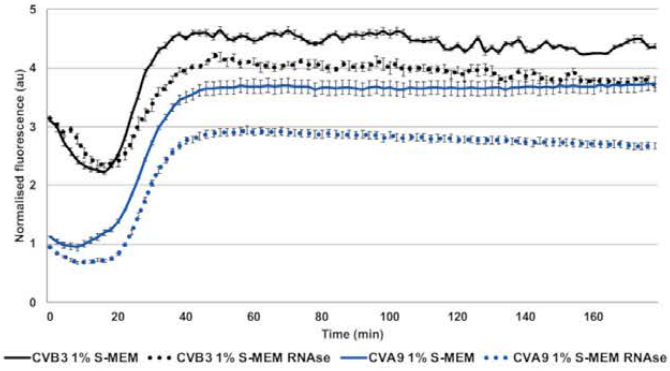

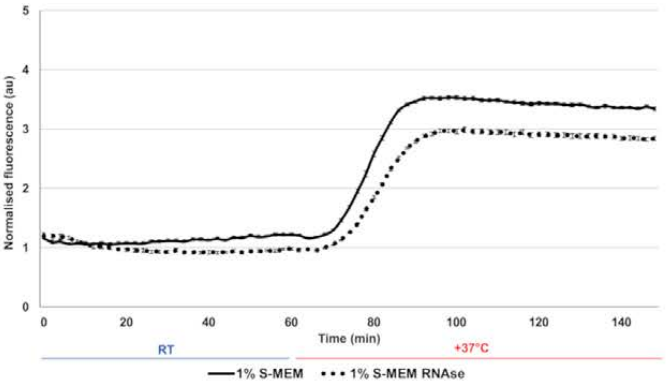

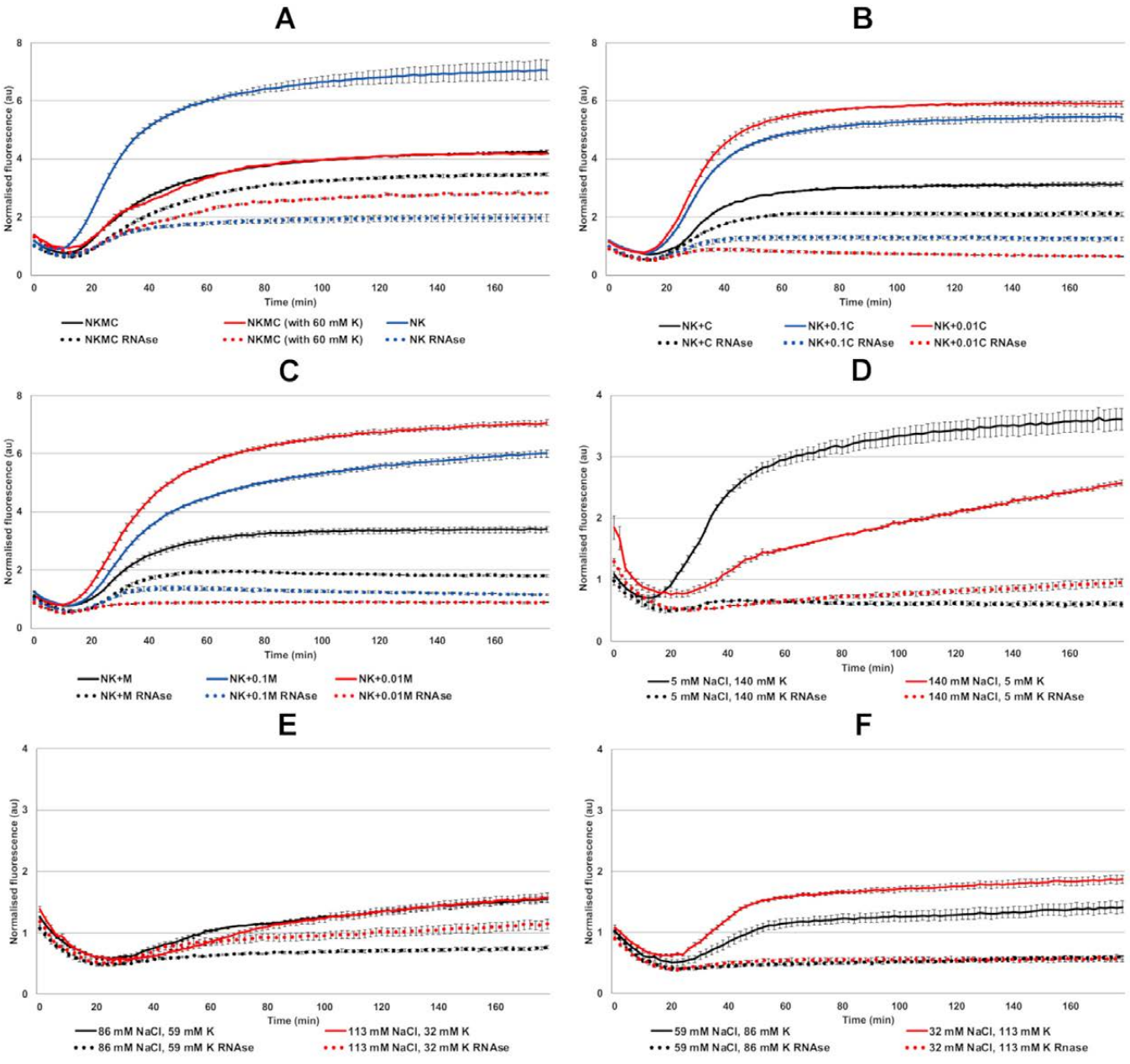

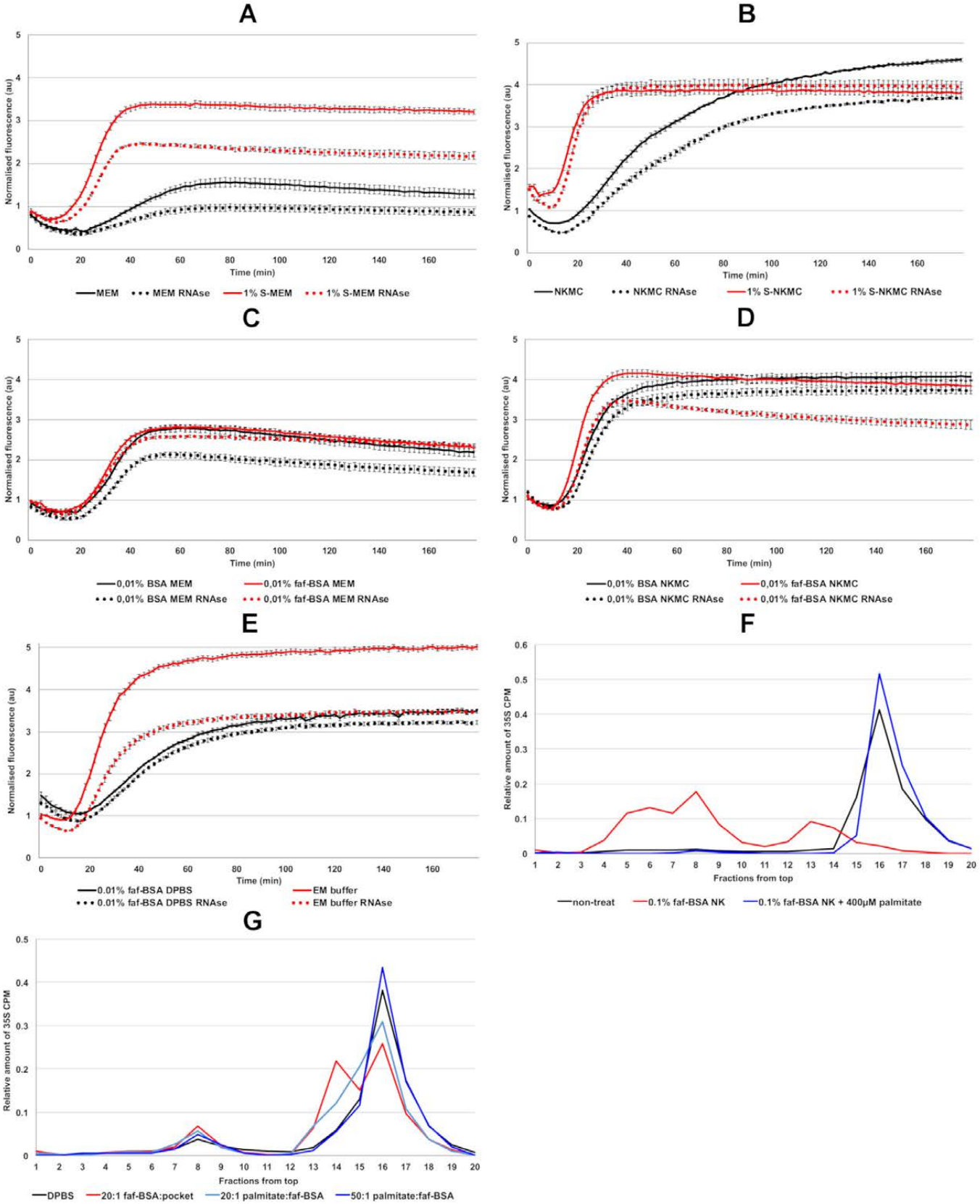

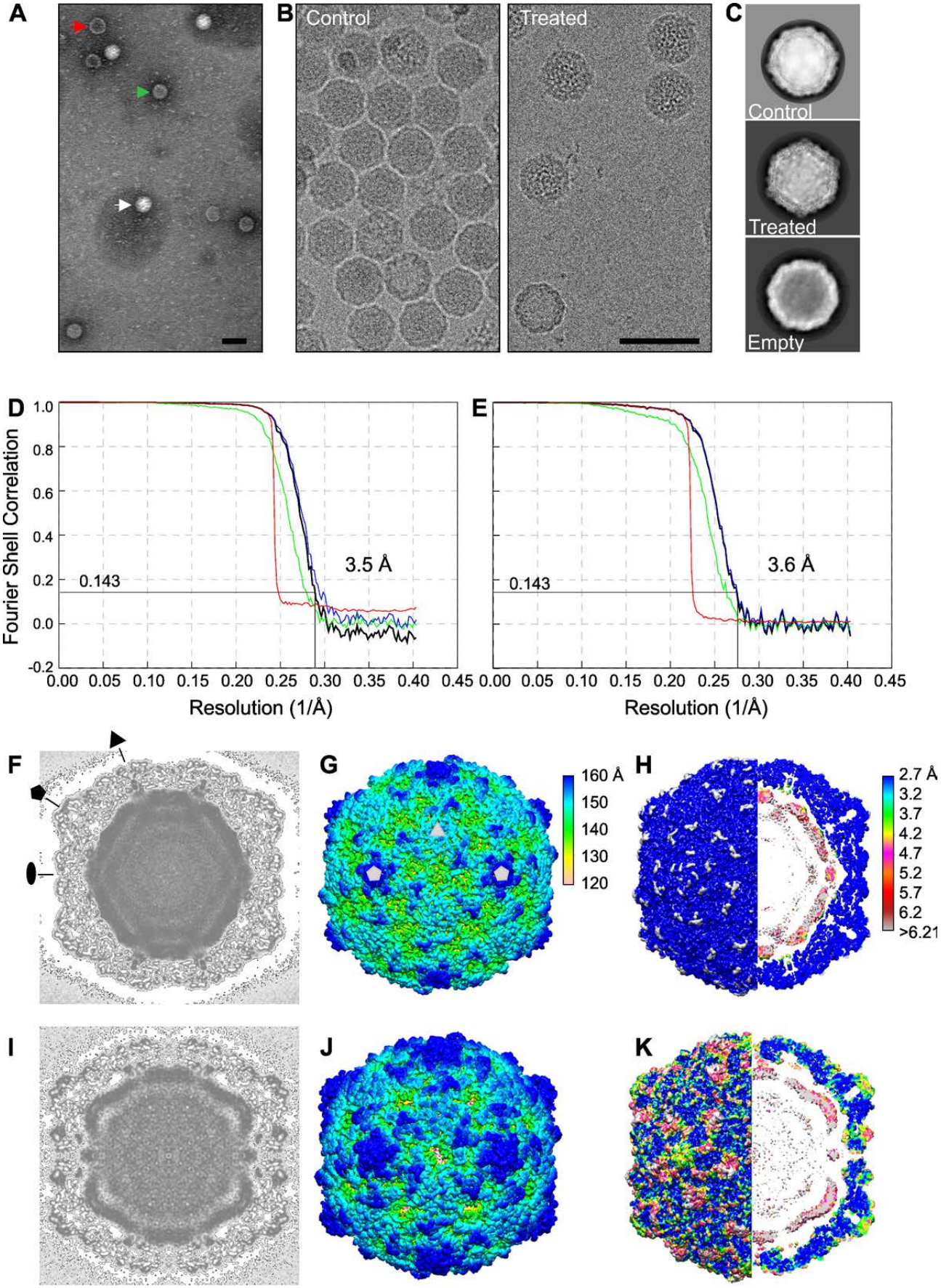

Journal of Virology